Aerodynamic Design Study of an Advanced Active Twist Rotor

Martin K. Sekula
martin.k.sekula@nasa.gov

Matthew L. Wilbur
matthew.l.wilbur@nasa.gov

William T. Yeager, Jr.
william.t.yeager@nasa.gov

U.S. Army Vehicle Technology Directorate
NASA Langley Research Center
Hampton, VA 23681

An Advanced Active Twist Rotor (AATR) is currently being developed by the U.S. Army Vehicle Technology Directorate at NASA Langley Research Center. As a part of this effort, an analytical study was conducted to determine the impact of blade geometry on active-twist performance and, based on those findings, propose a candidate aerodynamic design for the AATR. The process began by creating a baseline design which combined the dynamic design of the original Active Twist Rotor and the aerodynamic design of a high lift rotor concept. The baseline model was used to conduct a series of parametric studies to examine the effect of linear blade twist and blade tip sweep, droop, and taper on active-twist performance. Rotor power requirements and hub vibration were also examined at flight conditions ranging from hover to $\mu = 0.40$. A total of 108 candidate designs were analyzed using the second-generation version of the Comprehensive Analytical Model of Rotorcraft Aerodynamics and Dynamics (CAMRAD II) code. The study concluded that the vibration reduction capabilities of a rotor utilizing controlled, strain-induced twisting are enhanced through the incorporation of blade tip sweep, droop, and taper into the blade design, while they are degraded by increasing the nose-down linear blade twist. Based on the analysis of rotor power, hub vibration, and active-twist response, a candidate aerodynamic design for the AATR consisting of a blade with -10º of linear blade twist and a blade tip design with 30º sweep, 10º droop, and 2.5:1 taper ratio over the outer five percent of the blade is proposed.

Notation

$c_{0.95R}$	chord length at the 95% rotor radius, in
c_{tip}	chord length at the rotor tip, in
μ	advance ratio
θ_{tw}	Linear blade twist angle, positive leading edge up, deg
ρ_{air}	air density, slugs/ft^3
σ	rotor solidity
AATR	Advanced Active Twist Rotor
ATR	Active Twist Rotor
C_L	Rotor lift coefficient
C_X	Rotor drag coefficient
FRF	Frequency Response Function
HLR	High Lift Rotor
MFC	Macro Fiber Composite
N	Blade number
P	frequency (per revolution)
PFC	Piezoelectric Fiber Composite
R	Rotor radius, in
TDT	Transonic Dynamics Tunnel
TR	Taper ratio
Δ	Tip droop angle, positive down, deg
Λ	Tip sweep angle, positive aft, deg
Ω	Rotor angular velocity, rad/s

Presented at the American Helicopter Society 4th Decennial Specialist's Conference on Aeromechanics, San Francisco, California, January 21-23, 2004.

Introduction

In 1997, a cooperative effort between the NASA Langley Research Center, the Army Research Laboratory, and the MIT Active Materials and Structures Laboratory was developed to perform initial feasibility and proof-of-concept studies of active-twist rotor (ATR) technologies. The ultimate goals of the ATR program were to provide a wind-tunnel demonstration of an active-twist rotor concept that uses piezoelectric fiber composite (PFC) actuators[1-10] embedded in the blade skin, to investigate the potential benefits of such a system to reduce rotorcraft vibration and noise, and, to a lesser extent, to investigate potential improvements in rotor performance. This demonstration was first accomplished using a four-bladed, 110-inch diameter aeroelastically-scaled wind-tunnel model rotor designed for testing in the heavy gas, variable density test medium of the NASA Langley Transonic Dynamics Tunnel (TDT).[12] The TDT is a unique facility that permits full-scale rotor tip Mach numbers, Froude numbers, and Lock numbers to be matched simultaneously at model scale. In particular, the reduced speed of sound in the heavy gas test medium allows full-scale tip Mach numbers to be matched at lower rotational speeds and drive motor power.

References 3 through 6 document the design, fabrication, and bench and hover testing of a single

Active Twist Rotor prototype blade. Subsequently, a full set of ATR blades was fabricated and forward-flight testing was conducted in the TDT to assess the impact of active blade twist on rotating- and fixed-system vibratory loads, rotor performance, and acoustic noise generation. The results of a test examining open-loop vibration reduction are presented in references 7 and 8. References 9 and 10 present vibration reduction results using closed-loop active-twist control, with reference 10 also examining the impact of active-twist on rotor performance. An overview of the noise reduction capability is available in reference 11.

Based on the success of the wind-tunnel tests, recent improvements in PFC strain-actuation capacity, specifically the development of Macro-Fiber Composite (MFC) actuators,[12] and the encouraging results of the analytical modeling effort presented in reference 8, the design of a next generation active twist rotor, the Advanced Active Twist Rotor (AATR), was initiated. The original ATR was a proof-of-concept program, where the impetus driving the blade design (a rectangular blade planform and a NACA 0012 airfoil) was the reduction of design complexity.[3] The new AATR design will exploit current trends in blade design, such as advanced blade tips and high performance airfoils, to demonstrate that the active-twist concept can be successfully applied to a modern rotor. A further objective of this effort is to increase the active-twist control authority over that of the ATR, while improving the unactuated performance of the rotor by reducing rotor power and vibration.

This paper will focus on some of the issues related to the aerodynamic design of the AATR. In particular, it will discuss a series of five studies that examined how blade geometry can be altered to increase the blade active-twist control authority and to reduce unactuated rotor power and vibration. The goal of the first study was to gain an understanding of how blade geometry affects the blade torsion response which influences the blade active-twist control authority. Four more studies were conducted, each at a different advance ratio, with the goal of providing trends concerning the impact of various blade geometric parameters on rotor power and hub vibration of an unactuated rotor. Based on the results of these studies a candidate design for the AATR is proposed. These results will also indicate whether or not the design criteria for a successful active-twist rotor are contrary to those of a high-performance unactuated rotor.

Approach

The AATR is envisioned as a state-of-the-art helicopter rotor with excellent unactuated performance (low hub vibration and rotor power), further enhanced by active-twist technology. The design approach made use of an existing high-performance aerodynamic design in a series of parametric studies using the second-generation version of the Comprehensive Analytical Model of Rotorcraft Aerodynamics and Dynamics (CAMRAD II)[14] code. These studies assessed the impact of various blade design variables on blade torsion response, rotor power, and hub vibration at various flight conditions. The blade design chosen as a starting point for this study was a high-lift rotor (HLR) concept developed by U.S. Army Aviation and Missile Command personnel and tested at the TDT. Since this rotor proved too stiff for active-twist applications, the structural properties (dynamic design) of the original ATR were adopted. The resulting hybrid design uses the planform of the HLR, including hinge and pitch bearing locations, with the structural properties of the ATR modified to account for changes to the blade root and tip design. Although the differences in the ATR and HLR cross-sectional geometries and planforms may make it difficult to manufacture a HLR blade possessing the exact structural properties of the ATR, the union of these two designs is a good starting point for the design of the AATR.

The primary goal of the design study was to assess the impact of blade geometric properties on blade torsion response, rotor power, and hub vibration. Two major modeling assumptions were made to facilitate the analysis. First, it was assumed that the blade structural properties were independent of the blade geometric properties and remained constant along the blade span. The second simplifying assumption placed the chordwise center of gravity, elastic axis, and tension center at the local blade section quarter chord. The relative location of the tip quarter chord (and therefore the structural axes) was modified to reflect changes in blade dynamics associated with tip sweep and droop.

The HLR blade has a section with a constant chord length starting at 0.2489R and ending at 0.95R, where the tip sweep and taper commence. The AATR design calls for MFC actuators to be embedded in this constant chord portion of the blade. Since CAMRAD II currently does not have the capability to model voltage induced strains, the actuators were represented by two torsion moments, producing equal but opposing loads, applied to the blade at 0.2489R and 0.95R radial locations. The magnitudes of these moments were selected based on experimental values measured during ATR tests.

The aerodynamic model used throughout the study consisted of 19 aerodynamic panels spanning 0.1644R to 1.0R blade locations whose width decreased as the

blade tip was approached. A general method free-wake model was employed to capture rotor wake effects, where the far wake rollup was calculated using a single peak model with its strength based on the maximum magnitude of the blade circulation.

Using the above CAMRAD II model, a design study was conducted to examine the impact of rotor blade geometry on blade response, hub vibration, and rotor power. Linear blade twist and the sweep, droop, and taper ratio $\left(\frac{c_{0.95R}}{c_{tip}} : 1 \right)$ of the outboard five percent of the blade span were varied as part of the design and sensitivity study. In an effort to reduce the computational cost, three values of tip sweep, tip droop, and linear blade twist and four tip taper ratios spanning "typical" design values were chosen. Table 1 provides the values examined for the four blade geometry parameters, resulting in 108 variations of blade geometry that were investigated.

Table 1. Blade geometry parameter values.

Parameter	Linear Twist (deg)	Sweep (deg)	Droop (deg)	Taper Ratio
Value	-6, -10, -14	0, 15, 30	0, 10, 20	2.5:1, 1.67:1, 1.25:1, 1:1

Active-Twist Response

In order to exploit the active-twist concept to its fullest potential, it is apparent that a good understanding is required of the effect that blade geometry has on torsional response. The potential impact that each design variable may have on the torsion frequency response function (FRF) was determined by systematically analyzing the response functions of the 108 blade configurations. This was accomplished by actuating each blade planform using the two torsion moment representation of the MFCs and examining the blade torsion response at the 0.95R radial location. A comparison of the tip response would have been inappropriate since sensor location and possibly the coordinate system would change as a result of the blade tip sweep and droop variation.

Figure 1 shows the magnitude plots of the 0.95R torsion FRFs of all 108 blade geometries examined in this study. As shown, changes in the blade geometry can result in significant variations of the shape and magnitude of the blade torsion FRF. Upon closer examination, the maximum torsion response of the blade at the 0.95R location can vary from 2.9º (for a 0º sweep, 0º droop, 1:1 taper ratio, and -14º twist planform) to 4.3º (for a 30º sweep, 20º droop, 2.5:1 taper ratio, and -6º twist planform). In general, from an

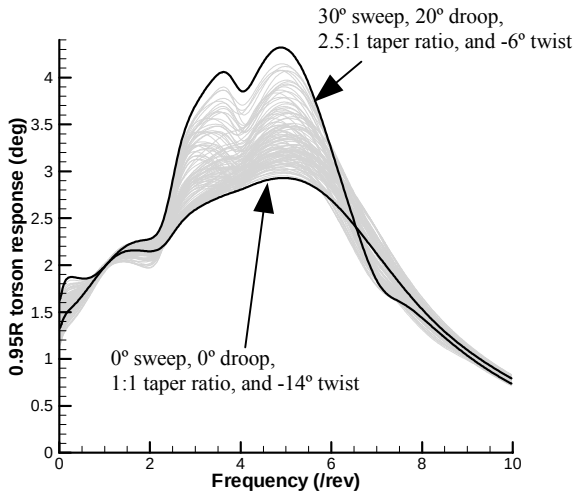

Figure 1. Variation in 0.95R torsion frequency response due to blade geometry changes.

active-twist standpoint, it is beneficial to increase the blade torsion response in the (N-1)P to (N+1)P region since the change in response magnitude is associated with the achievable amount of active-twist control authority for reducing hub loads. The current study examines a 4-bladed rotor (N = 4), therefore, increasing the torsion response in the 3P to 5P frequency range is of particular importance.

The impact of each blade geometric variable on the torsion FRF, and therefore the active-twist control authority, was determined by comparing the torsion FRFs of similar blade designs. Plots comprised of the FRFs of blade designs with only one varying geometric parameter were examined to determine the trends of how each parameter affects the torsion response. The results of the entire analysis are discussed below, but for sake of brevity, only a subset of the plots used to determine these trends are presented to provide a representative sample of the results. (See Figures 2 through 5.)

Changes in blade tip sweep had a significant impact on the torsion FRF. Figure 2 shows a typical variation in the torsion FRF created by changes in blade tip sweep while keeping the other parameters constant. As the tip sweep angle became larger, the torsion FRF tended to increase in magnitude, particularly in the 3P to 6P range. The resulting increase in torsion response occurred because the sweep angle introduced an aft, chord-wise shift of the CG location at the blade tip. This created a flap-torsion coupling exploiting the relatively large blade flap response to increase the torsion response.

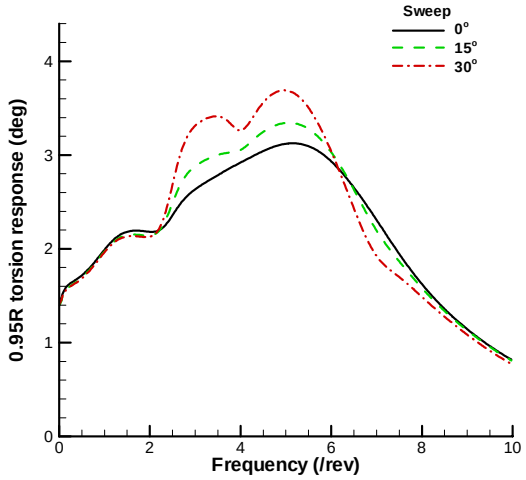

Figure 2. Sample change in torsion frequency response due to change in blade tip sweep, (0º droop, 1.67:1 taper ratio, -10º twist).

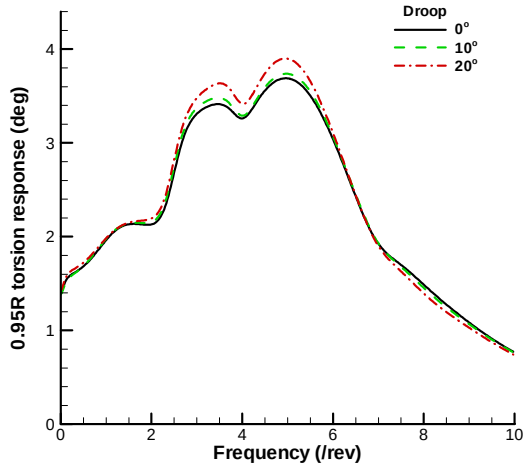

Figure 3. Sample change in torsion frequency response due to change in blade tip droop, (30º sweep, 1.67:1 taper ratio, -10º twist).

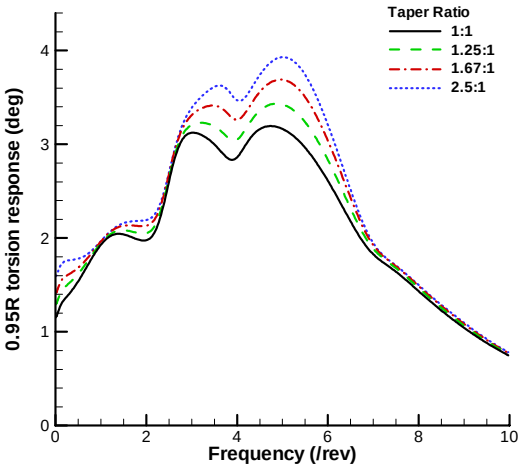

Figure 4. Sample change in torsion frequency response due to change in blade tip taper ratio, (30º sweep, 0º droop, -10º twist).

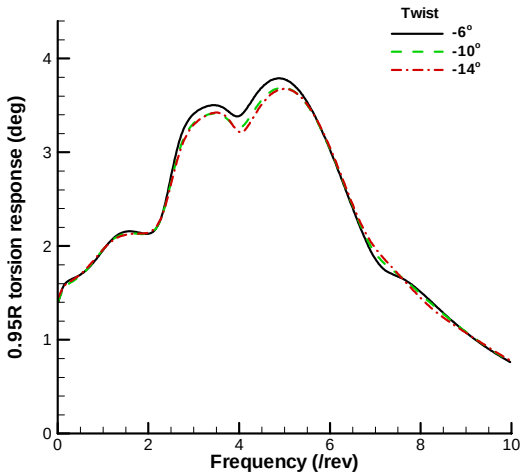

Figure 5. Sample change in torsion frequency response due to change in blade linear twist, (30º sweep, 0º droop, 1.67:1 taper ratio).

Figure 3 shows the typical effect of tip droop on the torsion FRF. The introduction of tip droop increases the torsion response in a manner similar to that resulting from tip sweep. Tip droop produces a lag-torsion coupling by shifting the tip CG out of the plane of the rotor disk. This coupling is smaller than the flap-torsion coupling produced by sweep, because blades are significantly stiffer in the lag degree of freedom.

Increasing tip taper ratio tended to produce an increase in torsion response, as shown in Figure 4. A thorough examination of the plots showing varying tip taper ratio revealed that the magnitude of the change in torsion response was dependent on the tip sweep angle, where greater sweep angles resulted in larger changes in response. In the current model, tip taper changed the planform area without affecting the tip mass, suggesting that the resulting increase in torsion response is caused by reduced aerodynamic damping. An examination of the blade eigenvalues revealed that the real components, or the modal damping, decreased with increasing taper ratio. It should be noted that tip taper should have less influence on the torsion FRF once a reduction in tip mass corresponding to the change in tip geometry is included in the analysis thereby decreasing the flap-torsion (and lag-torsion) coupling.

Blade linear twist was the only parameter examined which caused a small decrease in torsion response as its magnitude was increased. (See Figure 5.) The cause of this decrease is uncertain, although small increases in modal damping were observed.

In summary, increasing tip sweep, droop, and taper ratio generally results in a larger blade torsion response, while increasing nose-down blade linear twist decreases the response slightly. These observations are further substantiated by Figure 1 where the rotor blade configuration with the smallest maximum torsion response consisted of a 0º sweep, 0º droop, 1:1 taper ratio, and -14º twist blade planform, while a 30º sweep, 20º droop, 2.5:1 taper ratio, and -6º twist design exhibited the largest torsion response.

Performance Analysis

The impact of each blade parameter on rotor performance was assessed by trimming each blade configuration at several advance ratios and comparing the 4P vertical hub force magnitude (assumed to be representative of overall hub vibration) and rotor power to those of all other blade designs. Four flight conditions were examined (advance ratios of 0.0, 0.14, 0.30, and 0.40) representing flight speeds ranging from hover to high-speed flight. At each advance ratio, all rotor configurations were trimmed to identical lift and drag coefficients to provide a basis for comparing rotor performance. The rotor lift and drag were scaled to equivalent model values based on an 18,500 lb helicopter with a flat-plate area of 29.94 ft^2, a 26.8 ft rotor radius, Ω=27.05 rad/s, σ = 0.101, and $\rho_{air}=2.0482\times10^{-3}$ slugs/ft^3; a high altitude standard atmosphere flight condition. During analysis setup, it was assumed that the changes in $\frac{C_L}{\sigma}$, $\frac{C_X}{\sigma}$, and σ due to tip taper ratio produced relatively minor changes in trim, hub vibration, and rotor power, and therefore were kept constant for all blade designs in the CAMRAD II input file. This assumption was examined for several flight conditions and planforms and proved to be valid for the scope of this study.

The analysis was performed by plotting each trimmed rotor solution as a data point on a 4P vertical hub force versus rotor power plot. (See Figures 6 through 9.) At each advance ratio, the corresponding plots present identical results, but the symbols representing the data points are varied to present groups of constant sweep, droop, linear twist or taper ratio. This plotting strategy provided a simple method to determine the effect each parameter has on rotor power and hub vibratory loads. To clearly present the trends in each figure, several sets of data points representing similar blade configurations are highlighted. The values of the constant parameters in each highlighted data set are also provided, including arrows showing the direction of change in rotor power and vibration due to increasing parameter values.

Hover, μ = 0.0

In hover, the 108 rotor configurations were trimmed to a target $\frac{C_L}{\sigma}$ value of 0.0756. The comprehensive analysis does not predict any substantial vibratory loads in hover since the blades were assumed to be identical. Figures 6(a-b) present the 4P vertical hub force magnitude versus rotor power for all blade designs while grouping them by tip taper ratio and linear blade twist values, respectively. The figures presenting the variations in tip sweep and droop angles did not show any discernible effect on power and therefore are not presented. Increasing the taper ratio generally resulted in higher rotor power, shown in Figure 6a. Blade twist (Figure 6b) on the other hand, reduced rotor power as the nose-down blade twist angle increased, because these larger twist values should more closely approximate an ideal twist distribution for the required lifting task. A twist angle of -6º generally displayed power requirements 2 to 2.5 percent higher than the planforms with -10º and -14º of twist, which have very similar power requirements, within 0.3 percent of each other.

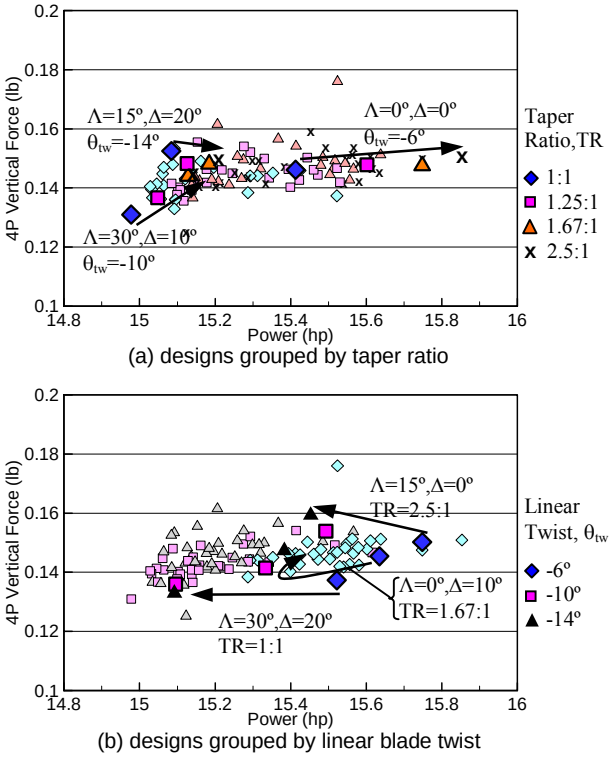

Figure 6. 4P hub vertical force vs. rotor power in hover, $\mu = 0.0$.

Low Speed Flight, $\mu = 0.14$

At an advance ratio of 0.14, all rotor configurations were trimmed using wind tunnel trim to lift and drag coefficients of $\frac{C_L}{\sigma}$ = 0.0756 and $\frac{C_X}{\sigma}$ = -0.001287. Figures 7(a-d) present 4P hub vertical force versus rotor power plots for all 108 blade geometries grouped by constant values of the various parameters. At this advance ratio, the effect of tip sweep and droop on power and vibration is heavily influenced by blade twist. Figure 7a indicates that incorporating sweep into rotors with small blade twist angles (-6º) results in an increase in rotor power and a small increase in hub vibration. Blade configurations with -10º of blade twist reduce rotor power but produce a small increase in vibration with increasing tip sweep, while increasing tip sweep in blade designs with large blade twist angles (-14º) is beneficial in reducing both the rotor power and hub vibration. The effect of tip droop on hub vibration also varies with twist angle, as shown in Figure 7b. For small twist angles (-6º), tip droop increases hub vibration, while when coupled with larger twist angles (-10º and -14º) tip droop reduces vibration.

Figure 7c presents the impact of tip taper on vibration and power. Unlike tip sweep and droop, its effects on power and vibration are insensitive to blade twist angle. For each blade configuration (constant tip sweep, droop, and linear blade twist), increasing the tip taper ratio decreases the rotor power by up to 0.1 hp or approximately 1 percent. The 4P hub vertical force decreases slightly with increasing taper.

Linear blade twist, presented in Figure 7d, has the most significant and clear impact on rotor vibration and power. Large twist angles tend to reduce rotor power as well as the 4P vertical hub force, while the small blade twist angle, -6º, show a large increase in both power and vibration, for this low speed case.

Cruise, $\mu = 0.30$

Figures 8(a-d) present 4P hub vertical force versus rotor power plots for all 108 blade geometries trimmed at an advance ratio of 0.30. All rotor configurations were trimmed to lift and drag coefficient values of $\frac{C_L}{\sigma}$ = 0.0756 and $\frac{C_X}{\sigma}$ = -0.005910 using wind tunnel trim. Tip sweep variation, Figure 8a, shows a decrease in vibration and power as tip sweep is increased. This is, in all likelihood, due to alleviation of compressibility effects since the tip Mach number on the advancing side is approaching 0.82. Figure 8b indicates that increasing

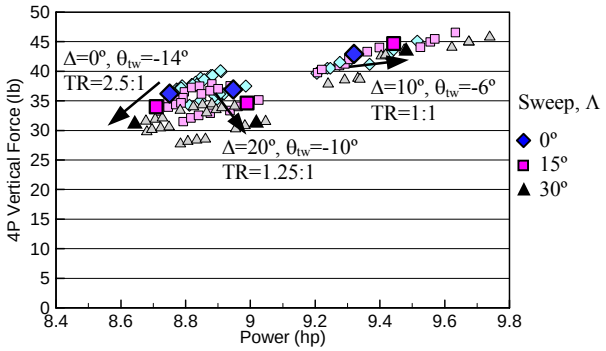

(a) designs grouped by tip sweep

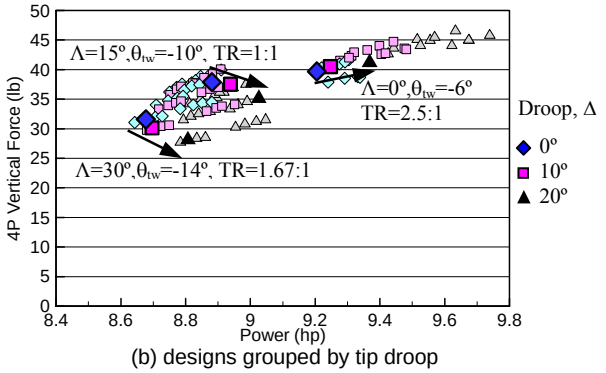

(b) designs grouped by tip droop

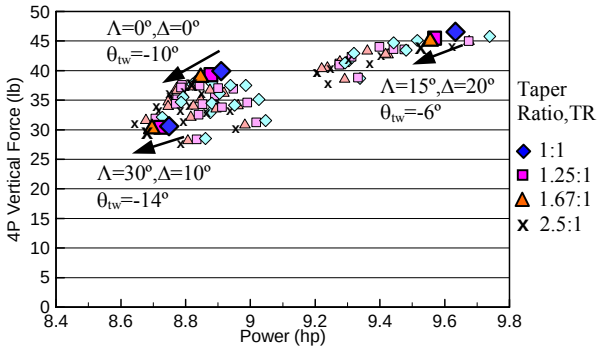

(c) designs grouped by taper ratio

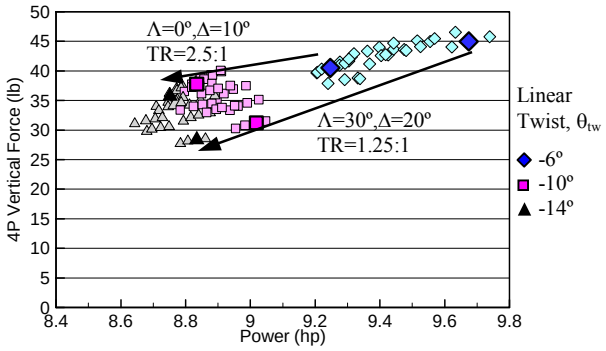

(d) designs grouped by linear blade twist

Figure 7. 4P hub vertical force vs. rotor power, $\mu = 0.14$.

the blade tip droop angle reduces rotor vibration while driving up rotor power.

The effect of blade tip taper on rotor power and hub vibration for a trimmed flight condition is shown in Figure 8c. Rotor power consistently showed a reduction of up to 0.2 hp (approx. 1.5%) due to increasing tip taper regardless of blade configuration (i.e. sweep, droop, and blade twist combinations.) Figure 8c indicates that the effect of taper ratio on hub vibration is influenced by tip sweep angle. For an unswept tip, hub vibration tends to reduce slightly (5-8%) when the tip taper ratio was increased from 1:1 to 2.5:1. Conversely, the same change in taper ratio increased hub vibration by 5 to 15 percent for blade designs with 30º of tip sweep. Blade configurations with 15º of tip sweep generally resulted in small (<3%) increases in vibration with changing tip taper.

Figure 8d indicates that increasing the nose-down blade twist results in higher 4P vertical vibration. The plot also indicates that rotor power is minimized by a linear blade twist of approximately -10º for all blade configurations.

High Speed Flight, $\mu = 0.40$

The results of the high-speed flight study, at an advance ratio of 0.40, are presented in Figures 9(a-d). The rotor configurations were trimmed using wind tunnel trim to lift and drag coefficient values of $\frac{C_L}{\sigma}$ = 0.0756 and $\frac{C_X}{\sigma}$ = -0.01051. Compared to advance ratio of 0.30, the average rotor power has substantially increased from approximately 11.8 hp to 20.4 hp. This increase can be partially attributed to the onset of retreating blade stall as well as drag divergence on the advancing side of the rotor disk, since the tip Mach number is approaching 0.88.

Figure 9a indicates that increasing the tip sweep angle decreased the rotor power in all the blade configurations considered by this study. This suggests that tip sweep alleviates some of the penalties associated with Mach number effects. However, the results do not exhibit any apparent trends relating changes in hub vibration to variations in tip sweep.

Figure 9b presents results grouped by tip droop angle. As shown, vibratory loads are generally insensitive to changes in tip droop, however, rotor power required tends to increase by as much as 4% as tip droop is increased.

The effects of blade tip taper variation are presented in Figure 9c. The results of the comprehensive

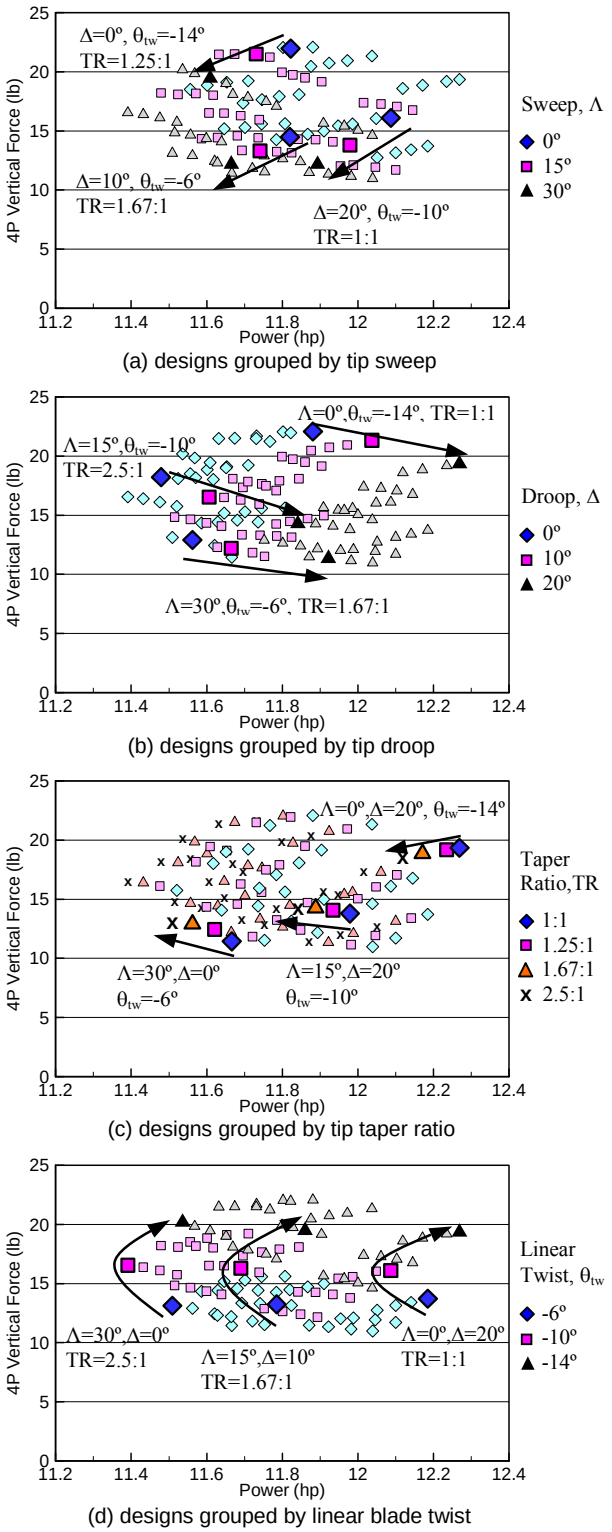

Figure 8. 4P hub vertical force vs. rotor power, $\mu = 0.30$.

aeroelastic analysis consistently show a reduction in rotor power caused by increasing the tip taper, regardless of blade configuration. These power reductions (due to changes from a rectangular tip to one with a 2.5:1 taper ratio) can be as much as 0.25 hp, greater than 1 percent of total power. The effect of tip taper on rotor vibration is highly coupled with the tip sweep angle. Figure 9c indicates that increasing the taper ratio in an unswept tip reduced the 4P vertical hub force by up to 14 percent. In a blade configuration with 15º of blade sweep, hub vibration generally was slightly reduced by tip taper. But, for blade designs with 30º of tip sweep, hub vibration increases by up to 23 percent when tip taper was incorporated into the design.

Figure 9d shows the effect of linear blade twist on rotor power and 4P vertical hub force. Increasing the nose-down blade twist drove hub vibration up significantly, while -10º of twist tended to minimize rotor power.

Rotor Blade Planform Selection

The methodology used to select the best candidate blade planforms for the AATR is presented below. For the purpose of this investigation, it is assumed that obtaining the most favorable values for the 4P vertical hub force, rotor power, and blade torsion response are the most important objectives. The planform selection process began by examining the results of the parametric studies discussed in the previous sections. One of the major objectives of this study was to design a rotor exhibiting low hub vibration and rotor power during unactuated operation. Therefore, at each of the four advance ratios, blade configurations exhibiting high rotor power or large vibration were eliminated from consideration. The remaining blade designs from each advance ratio were examined to determine common designs exhibiting desirable performance characteristics at all flight speeds. The final selection of the AATR aerodynamic blade design was determined by examining the potential active-twist capability of the down-selected designs. Blade configurations exhibiting large torsion response in the 3P to 5P frequency range were considered to be the most desirable to achieve the maximum vibration reduction control authority, making this the criteria for the final selection of potential AATR designs.

Hover and cruising flight performance were examined first since it was assumed that a typical helicopter would spend a majority of its flight time at these two flight conditions. Therefore, identifying blade designs with good performance characteristics at both conditions was of primary concern. Examination of the 4P vertical hub force versus power plots for hover, Figures 6(a-b), reveal that planforms with -6º of twist require higher

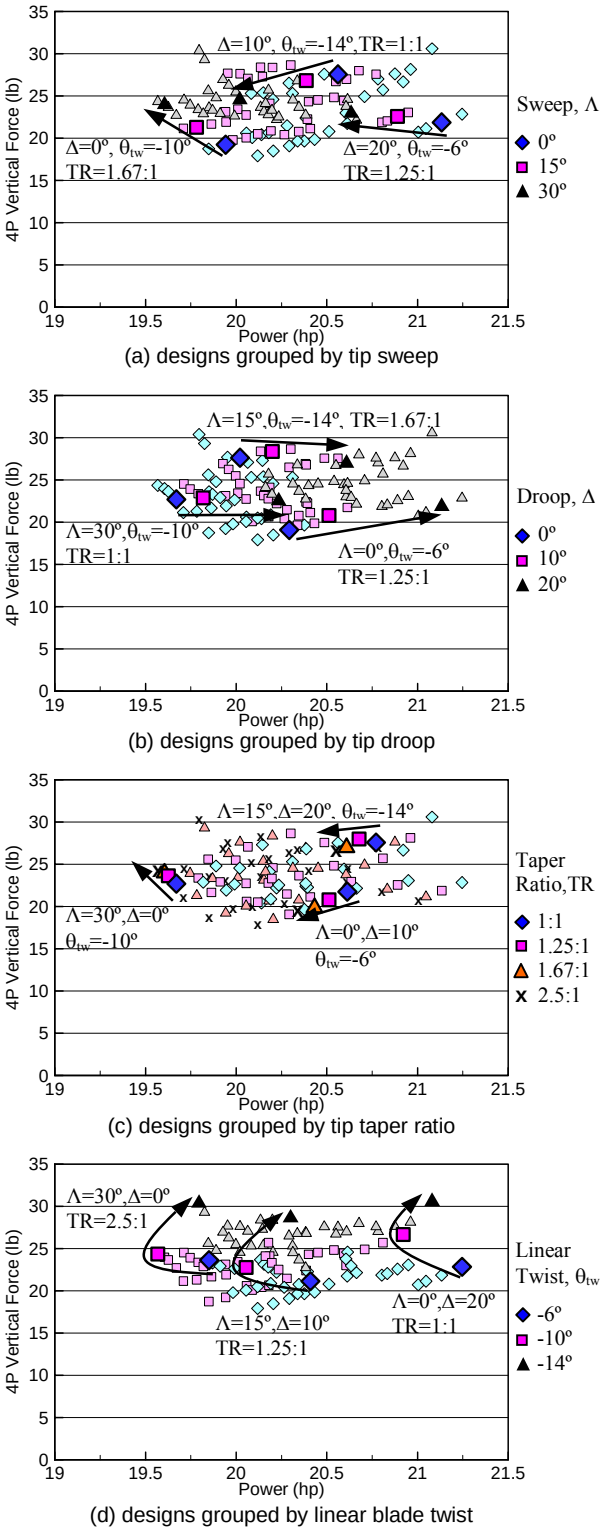

Figure 9. 4P hub vertical force vs. rotor power, $\mu = 0.40$.

rotor power than configurations with other blade twist angles. Therefore, blade designs with -10º and -14º of blade twist are most desirable based on hover performance considerations. At an advance ratio of 0.30, a series of planforms encompassing the lower left hand region of the results in Figures 8(a-d), representing low power and vibration, were chosen as candidate planforms. These 29 selected planforms are highlighted in Figure 10. It should be noted that Figure 10 indicates that blade designs with -14º of blade twist are not desirable due to high vibratory loads at the cruise advance ratio, $\mu = 0.30$. This is in direct contrast with optimal designs for hover. A comparison of the optimal designs for hover and cruise speed revealed 12 blade configurations common to both flight speeds. These became the candidate planforms for the AATR design based on low rotor power and hub vibration criteria for hover and cruising speed.

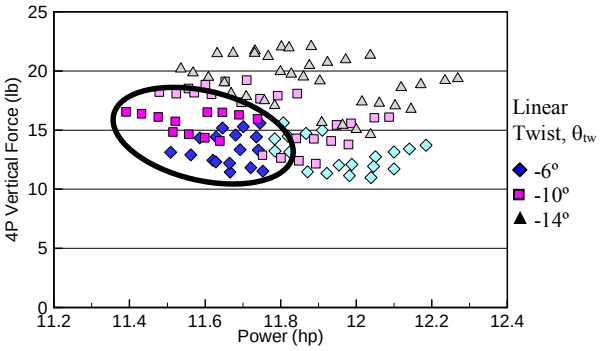

Figure 10. Low power and vibration planforms at $\mu = 0.30$.

The selection process continued by conducting a similar analysis of the low- and high-speed flight conditions, advance ratios of 0.14 and 0.40, to highlight designs that perform well in these flight regimes. Figure 7d, the effect of linear blade twist on rotor power and hub vibration at an advance ratio of 0.14, shows that blade twist had a major impact on rotor power and hub vibration. Blade designs with -10º and -14º of linear blade twist were preferred since they produced significantly lower rotor power and hub vibration than -6º blade twist designs at this flight condition. Of these, configurations with all 30º and some configurations with 15º tip sweep angles are most desirable since they produced the smallest hub vibration of all the tip designs (Figure 7a). At an advance ratio of 0.40, 20 planforms producing low power and vibration were selected from Figures 9(a-d), and are highlighted in Figure 11. Comparing the two lists of candidate designs for low- and high-speed flight with the configurations obtained through the hover and cruise selection process revealed nine planforms, presented in Table 2, that meet the low power and vibration requirements at all flight speeds.

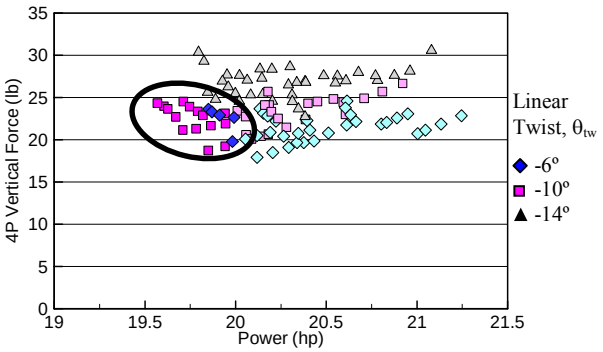

Figure 11. Low power and vibration planforms at $\mu = 0.40$.

Table 2. Low power and vibration planforms at all flight speeds.

Planform Number	Sweep, (deg)	Droop, (deg)	Taper Ratio	Twist, (deg)	Planform Number	Sweep, (deg)	Droop, (deg)	Taper Ratio	Twist, (deg)
1	15	10	2.5:1	-10	6	30	10	1:1	-10
2	30	0	1:1	-10	7	30	10	1.25:1	-10
3	30	0	1.25:1	-10	8	30	10	1.67:1	-10
4	30	0	1.67:1	-10	9	30	10	2.5:1	-10
5	30	0	2.5:1	-10					

As the final step in the down-selection process, the torsional response due to active-twist was evaluated. Figure 12 highlights the 0.95R torsion FRFs of the 9 blade designs presented in Table 2. The blade configurations with 30º tip sweep, -10º blade twist, 2.5:1 taper ratio, with either 0º or 10º of tip droop (shown as dashed lines) provided the largest torsion response, and therefore should result in the largest active-twist control authority.

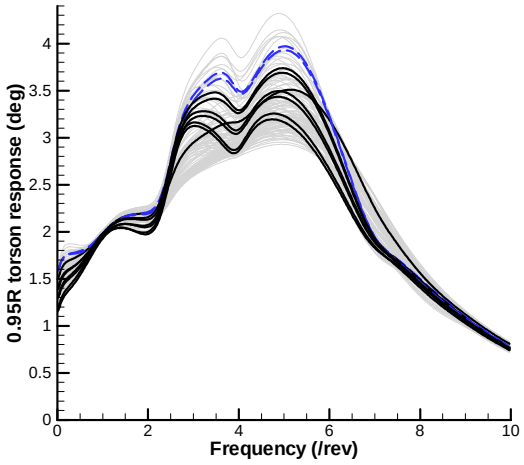

Figure 12. Torsion frequency response functions highlighting the 9 candidate planforms.

Analysis of Active-Twist Control Authority

An examination of the torsion FRFs in Figure 12 did not reveal a clear choice for the final blade design since two designs had comparable torsional responses. The final selection of the blade design was therefore made by directly examining the vibration reduction control authority of the two designs at an advance ratio of 0.30 ($\frac{C_L}{\sigma}$ = 0.0756 and $\frac{C_X}{\sigma}$ = -0.005910). Each design was evaluated using the same active-twist moment amplitude and frequency, while varying the phase angles to produce a response map. A rectangular planform representative of the original ATR configuration was also examined to gauge the potential improvement in vibration reduction over the original ATR. The study was further expanded to include a swept tip planform without taper (1:1 taper ratio) or tip droop in order to provide further detail to the study. The four cases examined were:

1. 0º sweep, 0º droop, 1:1 taper ratio, -10º twist; Rectangular (ATR)
2. 30º sweep, 0º droop, 1:1 taper ratio, -10º twist
3. 30º sweep, 0º droop, 2.5:1 taper ratio, -10º twist
4. 30º sweep, 10º droop, 2.5:1 taper ratio, -10º twist

This choice of planforms permitted a limited, systematic study examining the individual effects of tip sweep, droop, and taper on the active-twist control authority.

Figure 13 presents the response maps of the 4P vertical hub force for the four planforms discussed above. On this plot, the 4P vertical hub force is decomposed into its cosine and sine components which are plotted on the horizontal and vertical axes, respectively. The symbols represent the hub loads of the unactuated rotors, while the octagonal shapes surrounding the symbols represent the vibratory loads produced when each rotor was actuated using a 6 in-lb torsional actuation moment at a frequency of 3P. The active-twist responses presented were generated by varying the actuation phase angle from 0° to 315° in 45° increments. A radial line extends from the symbols representing the unactuated cases to indicate the vibration response due to active-twist at 0° control phase. The area encompassed by the octagonal vibration response region represents the active-twist control authority available. This indicates that any vibratory load within this region may be achieved using the proper combination of active-twist control phase and active-twist control moment of 6 in-lb or less.

Figure 13 indicates that the control authority gained through the addition of tip sweep, droop, and taper follows the same trends observed in the torsion frequency response function discussed previously. The

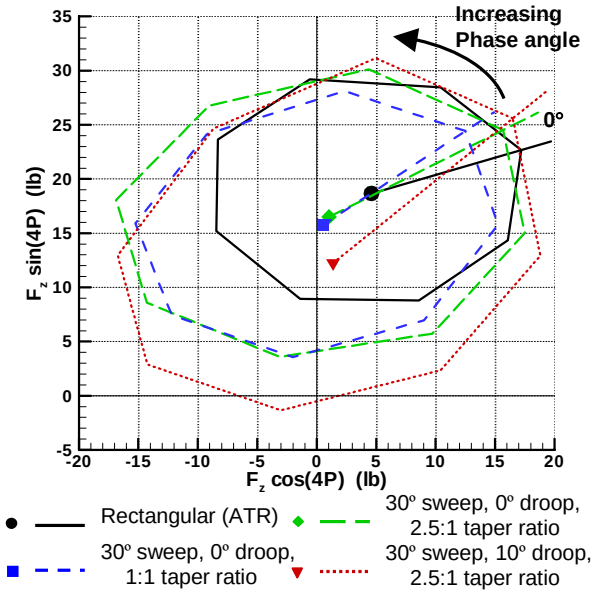

Figure 13. Response map of 4P vertical hub force for unactuated (shown with symbols) and actuated (shown with lines) response, 6 in-lb,3P actuation at 45º control phase increments, μ = 0.30.

addition of tip sweep to the rectangular planform not only decreased unactuated rotor vibration, but increased the radius of the response map, signifying an increase in active-twist control authority. The addition of tip taper had little effect on the unactuated vibratory loads, but it further increased the control autority of active-twist, just as tip taper increased the 0.95R maximum torsion response. The addition of 10º of tip droop, while not showing a large impact on the torsion FRF, significantly increased the radius of the response map. This increase in the size of the response map, combined with a reduction of the unactuated 4P vertical hub force resulted in a response map encompassing the origin, signifying the possibility of completely eliminating the hub load by actuating the blade at the correct phase angle with a moment slightly smaller than 6 in-lb.

Based on the results of the active-twist control authority analysis, the proposed AATR aerodynamic design has been selected. The AATR will be composed of a blade geometry with -10º of linear blade twist and a blade tip design with 30º sweep, 10º droop, and 2.5:1 taper ratio in the outer five percent of the blade. The shape of the AATR blade combining these design elements is presented in Figure 14.

Conclusions

The U.S. Army Vehicle Technology Directorate is currently developing a design for a second generation Active Twist Rotor, the Advanced Active Twist Rotor. The design process began with a hybrid blade design

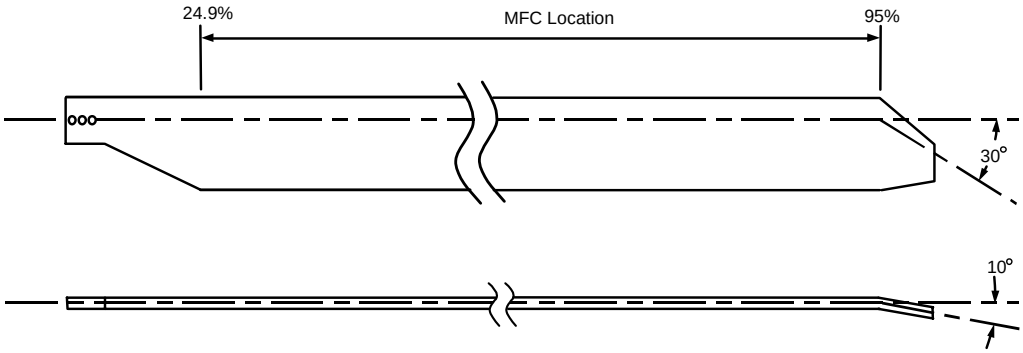

Figure 14. The planform of the proposed design for the Advanced Active Twist Rotor.

combining the planform geometry of a high-lift rotor concept and the dynamic design of the original Active Twist Rotor. Potential improvements to this baseline design were investigated analytically through a systematic examination of the impact of blade geometry on rotor power, hub vibration, and active-twist response using the CAMRAD II aeroelastic rotor analysis. Based on this effort, the following conclusions which apply only to this design were reached:

1. Blade torsion response is increased by integrating tip sweep, droop, and taper into the blade design, while increasing nose-down linear blade twist decreases the response.

2. Tip sweep and droop increased the torsion response by introducing a flap-torsion and a lag-torsion coupling, respectively. Blade tip taper increased the torsion response by reducing the aerodynamic damping of the blade modes.

3. Blade tip taper and linear blade twist were the only parameters examined which had a discernable impact on rotor power in hover. Increasing tip taper increased rotor power while larger values of nose-down blade twist reduced rotor power.

4. Tip sweep, in general, reduced rotor power at all forward flight conditions examined. At cruise speed flight, increasing sweep angles reduced rotor vibration. At low- and high-speeds, more complex trends in vibration were present.

5. At all forward flight speeds examined, tip droop consistently showed an increase in rotor power with increasing droop angles. Hub vibration was generally reduced by the introduction of tip droop at low-speed and cruise conditions, but the high-speed flight study did not reveal any apparent trends in vibration.

6. Increasing the tip taper reduced rotor vibration in low-speed flight, while in cruise and high-speed flight the effect of tip taper on vibration is dependent on the tip sweep angle. Rotor power was consistently reduced (approximately 1% for 2.5:1 taper ratio compared to 1:1 taper ratio) by increasing tip taper at all forward-flight speeds examined.

7. Increasing the linear blade twist in low-speed flight reduced both rotor power and hub vibration. At cruise and in high-speed flight, -10º of twist generally minimized rotor power while decreasing the nose-down twist would reduce hub vibration.

8. Active and unactuated design objectives proved not to compete with one another. In general, blade geometric parameters having a positive impact on unactuated blade performance also resulted in improvements in active-twist response and vibration reduction control authority.

Based on the above conclusions, the original hybrid design of the AATR was modified to include -10º of linear blade twist and a blade tip design with 30º sweep, 10º droop, and 2.5:1 taper ratio over the outer five percent of the blade. This design is a compromise providing a rotor design with low hub vibration and low rotor power throughout the entire flight-speed range for an unactuated rotor, while significantly improving the active-twist vibration reduction capabilities over those of the original ATR design.

References

1. Derham, R., Weems, D., Mathew, M., and Bussom, R., "The Design Evolution of an Active Materials Rotor," American Helicopter Society 57th Annual Forum Proceedings, Washington, DC, May 2001.

2. Rodgers, J. P., and Hagood, N. W., "Development of an Integral Twist-Actuated Rotor Blade for

Individual Blade Control," Active Materials and Structures Laboratory, AMSL Report #98-6, Massachusetts Institute of Technology, October 1998.

3. Wilkie, W. K., Wilbur, M. L., Mirick, P. H., Cesnik, C. E. S., and Shin, S. J., "Aeroelastic Analysis of the NASA/Army/MIT Active Twist Rotor," American Helicopter Society 55th Annual Forum Proceedings, Montreal, Canada, May 25-27, 1999.

4. Cesnik, C. E. S., Shin, S. J., Wilkie, W. K., Wilbur, M. L., and Mirick, P. H., "Modeling, Design, and Testing of the NASA/Army/MIT Active Twist Rotor Prototype Blade," American Helicopter Society 55th Annual Forum Proceedings, Montreal, Canada, May 1999.

5. Shin, S. J., and Cesnik, C. E. S., "Design, Manufacturing and Testing of an Active Twist Rotor," Active Materials and Structures Laboratory, AMSL Report #99-3, Massachusetts Institute of Technology, June 1999.

6. Wilbur, M. L., Yeager, W.T., Jr., Wilkie, W. K., Cesnik, C. E. S., and Shin, S. J., "Hover Testing of the NASA/Army/MIT Active Twist Rotor Prototype Blade," American Helicopter Society 56th Annual Forum Proceedings, Virginia Beach, VA, May 2000.

7. Wilbur, M. L., Mirick, P. H., Yeager, W. T., Jr., Langston, C. W., Cesnik, C. E. S., Shin, S. J., "Vibratory Loads Reduction Testing of the NASA/Army/MIT Active Twist Rotor," American Helicopter Society 57th Annual Forum Proceedings, Washington, D. C., May 2001.

8. Wilbur, M. L., Yeager, W. T., Jr., Sekula, M. K., "Futher Examination of the Vibratory Loads Reduction Results from the NASA/Army/MIT Active Twist Rotor Test," American Helicopter Society 58th Annual Forum Proceedings, Montréal, Canada, June 2001.

9. Shin, S. J., Cesnik, C. E. S., Hall, S. R., "Closed-Loop Control Test of the NASA/Army/MIT Active Twist Rotor For Vibration Reduction," American Helicopter Society 59th Annual Forum Proceedings, Phoenix, AR, May 2003.

10. Bernhard, A. P. F., Wong, J., "Sikorsky Active Rotor Control Evaluation of NASA/Army/MIT Active Twist Rotor," American Helicopter Society 59th Annual Forum Proceedings, Phoenix, AR, May 2003.

11. Booth, E. R. and Wilbur, M. L., "Acoustic Aspects of Active Twist Rotor Control," American Helicopter Society 58th Annual Forum Proceedings, Montreal, Canada, June 2002.

12. Wilkie, W. K., et. al., "Low-Cost Piezocomposite Actuator for Structural Control Applications," SPIE 7th Annual International Symposium on Smart Structures and Materials, Newport Beach, CA, March 2000.

13. Yeager, W. T., Jr., Mirick, P. H., Hamouda, M-N., Wilbur, M. L., Singleton, J. D., and Wilkie, W. K., "Rotorcraft Aeroelastic Testing in the Langley Transonic Dynamics Tunnel," Journal of the American Helicopter Society, Vol. 38, No. 3, July 1993, pp. 73-82.

14. Johnson, W., CAMRAD II, Comprehensive Anaytical Model of Rotorcraft Aerodynamics and Dynamics, Johnson Aeronautics, Palo Alto, California, 1994.